A numerical analysis of thermally developing flow in elliptic ducts with internal fins

Z. F. Dong and M. A. Ebadian
Department of Mechanical Engineering, Florida International University, Miami, FL, USA

The thermally developing laminar forced-convection flow and heat transfer characteristics in elliptic tubes with four longitudinal internal fins is numerically investigated in this article via the boundary-fitted coordinate system. The control volume-based finite-difference technique is applied to obtain the solution utilizing the numerically generated boundary-fitted coordinate. The elliptic tubes are maintained at a uniform wall temperature, peripherally as well as axially. Since the fins are considered to be continuous and of zero thickness, the results presented are in terms of isotherms, variation of bulk temperature, and Nusselt number in the entire thermal region of the elliptic duct for various values of relative fin heights. Also studied and graphically illustrated is the effect of minor-axis to major-axis ratios in the elliptic duct with internal fins on the fully developed and developing heat transfer characteristics. For the special case of a circular duct, the results are compared with some limited findings in the literature, and very good agreement is obtained. Furthermore, the results exhibit a high heat transfer coefficient, expected in the entrance region, approaching asymptotically fully developed values at greater axial distances. The significance of each curve is also discussed in detail.

Keywords: forced convection; numerical methods; heat exchangers; augmentation and enhancement; heat pipe and thermosyphon

Introduction

Longitudinal fins within ducts are often employed for the purpose of heat transfer augmentation. Such internally finned tubes find numerous applications in compact heat exchanger devices. A literature survey by Eckert,[1–4] Kakac,[5] Shah and London,[6] Soloukhin and Martynenko,[7] and Martynenkos indicates that significant attention has been devoted in recent years to the investigation of laminar fluid flow and heat transfer in internal finned tubes. However, these investigations are predominantly concerned with forced convection in the developing and fully developed region of the circular duct. Among these, Hu and Chang,[9] Nandakumar and Masliyah,[10] Soliman and Feingold,[11] Soliman,[12] Prakash and Liu,[13] and Rustum and Soliman[14] studied the uniform wall temperature and uniform wall heat flux boundary conditions. However, for noncircular geometries of elliptic ducts with longitudinal fins, knowledge of fluid flow and forced convection is absent in the open literature. Recently, an investigation of forced-convection heat transfer in the entrance region of the semicircular duct with internal fins subjected to a uniform wall temperature was published by Zhang et al.[15] They solved the three-dimensional (3-D) energy equation using the method of lines (MOL). Their results contained various relative fin heights, as well as different numbers of fins.

As in the case of convection heat transfer in the elliptic duct but without internal fins, there are only a few papers published in the open literature. For instance, Tao[16] and Schenk and Han" dealt with convective heat transfer for laminar flows in tubes of elliptic cross section maintained under constant heat flux. Ebadian[18] investigated convective heat transfer in an elliptic duct subjected to constant wall temperature. They solved for thermally fully developed laminar flow using the successive approximation method. Again, none of these investigations treats the augmentation of heat transfer using longitudinal internal fins. Therefore, the main objective of this article is to analyze the enhancement of convective heat transfer in the entrance region of the elliptic duct through the attachment of longitudinal internal fins. The duct is also subjected to constant wall temperature. Unlike the circular duct in which, in general, the effects of the number of fins is investigated, flow and heat transfer in the elliptic duct is mainly dependent on the location of internal fins. Thus, only four fins are chosen in this study, and they are located on the horizontal and vertical symmetry lines. Figure 1 illustrates the elliptic duct geometry with four internal fins. Three minor-axis to major-axis ratios of $\alpha^* = 0.25$, 0.5, and 0.8 are investigated in this article. The flow is considered to be laminar and the physical properties are also assumed to be constant. The developing temperature in these geometries is determined by solving the three-dimensional energy equation via the control volume-based finite-difference method, where the relative fin height as well as different minor-axis to major-axis ratios are included. Due to the complexity of the tinned elliptic duct geometry, the numerically generated boundary-fitted coordinate system is applied to discretize the computational domain. Accordingly, the governing equations are formulated in the boundary-fitted coordinate system and then are solved successively. In addition, an independent grid test is conducted to optimize the accuracy of the results obtained. Thus, the variation of isotherms, the bulk temperature, and the local Nusselt number is presented in the region of thermal development for different minor-axis to major-axis ratios and several relative fin heights. Also presented in this article are the results for the fully developed flow condition. For the special case of the circular duct in the region of thermal development, only two papers dealing with the same cross section, but without longitudinal tins, have been published

Address reprint requests to Professor Ebadian at the Department of Mechanical Engineering, Florida International University, Miami, FL 33199, USA.

Received 6 September 1990; accepted 25 October 1990

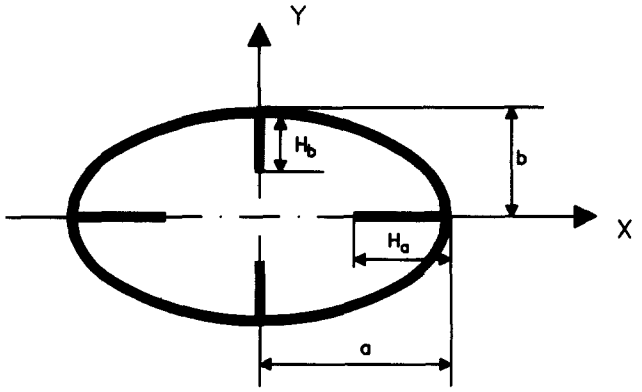

Figure 1 Fin tube geometry

(Shah and London[6] and Rustum and Soliman[14]). In this case, the result with no longitudinal fins is compared with the above-cited papers and an excellent agreement is obtained. For the special case of the circular duct, the variation of the local Nusselt number with internal fins has also been compared with the results of Rustum and Soliman,[14] and again, an excellent agreement between the two is obtained.

It is believed that availability of these solutions is important for the designer and practitioner in areas such as compact heat exchangers, turbines, etc.

Analytical formulation

The problem considered here is that of an elliptic duct, as shown in Figure 1. The elliptic duct has four fins that are distributed on the major and minor axes of the ellipse. The fins are assumed to be of zero thickness and with different relative fin heights. The flow in the duct is considered to be laminar and hydrodynamically fully developed, but thermally developing in the entrance region of the duct. The fluid is Newtonian with constant thermal properties. The governing equations in terms of dimensionless variables can be expressed as

Momentum Equation

$$\frac{\partial^2 W}{\partial X^2}+\frac{\partial^2 W}{\partial Y^2}+1=0 \tag{1}$$

Energy Equation

$$C\frac{\partial \theta}{\partial Z}=\left(\frac{\partial^2 \theta}{\partial X^2}+\frac{\partial^2 \theta}{\partial Y^2}\right) \tag{2}$$

where

$$C=\frac{W}{W_m}\left(\frac{a}{D_{\mathrm{hf}}}\right)^2 \tag{3}$$

where in the above equations, W represents the dimensionless velocity, θ the dimensionless temperature, D_{hf} the hydraulic

Notation

A Cross-sectional area, m^2
a Semi-major axis of elliptic duct, m
b Semi-minor axis of elliptic duct, m
C Coefficient, Equation 3
C_p Specific heat at constant pressure, $J\,kg^{-1}\,K^{-1}$
D_{hf} Hydraulic diameter of duct with fin, m
D_{hs} Hydraulic diameter of duct without fin, m
F Dependent variable, Equation 24
f Friction factor
H_a Fin height, m, Figure 1
H_b Fin height, m, Figure 1
H^* Relative height of fin, $\frac{H_a}{a}=\frac{H_b}{b}$
h Heat transfer coefficient, $W\,m^{-2}\,K^{-1}$
J Jacobian transformation, Equation 23
k Thermal conductivity, $W\,m^{-1}\,K^{-1}$
L_T Dimensional thermal entrance length, m
L_t^* Dimensionless thermal entrance length, $\frac{L_T}{D_{\mathrm{hf}}\mathrm{Re}\mathrm{Pr}}=\frac{L_T}{D_{\mathrm{hf}}^2 W_m \alpha^{-1}}$
n Outward normal direction on boundary
Nu Nusselt number, $\frac{hD_{\mathrm{hf}}}{k}$ or $\frac{hD_{\mathrm{hs}}}{k}$, Equations 12 and 13
P Perimeter, m
Pr Prandtl number, $\frac{\nu}{\alpha_T}$
p Pressure, $kN\,m^{-2}$
Re Reynolds number, $\frac{w_m D_{\mathrm{hf}}}{\nu}$ or $\frac{w_m D_{\mathrm{hs}}}{\nu}$
T Temperature of fluid, K
T_b Bulk temperature of fluid, K
T_i Inlet temperature of fluid, K
T_w Circumferential wall and fin temperatures, K
W Dimensionless velocity, $-\frac{\mu w}{a^2\frac{dp}{dz}}$
W_m Dimensionless mean velocity, $\frac{1}{A}\iint W\,dA$
w Velocity, $m\,s^{-1}$
w_m Mean velocity ($m\,s^{-1}$), $\frac{1}{A}\iint w\,dA$
X, Y Dimensionless transversal coordinates, $\frac{x}{a}, \frac{y}{a}$
x, y Dimensional transversal coordinates, m
Z Dimensionless axial coordinate, $\frac{z}{D_{\mathrm{hf}}\mathrm{Re}\mathrm{Pr}}$
z Dimensional axial coordinate, m

Greek symbols

α Coefficient, Equation 16
α_T Thermal diffusivity, $m^2\,s^{-1}$
α^* Minor-axis to major-axis of the elliptic duct
β Coefficient, Equation 17
γ Coefficient, Equation 18
ρ Density, $kg\,m^{-3}$
μ Dynamic viscosity, $kg\,m^{-1}\,s^{-1}$
ν Kinematic viscosity, $m^2\,s^{-1}$
θ Dimensionless temperature, $\frac{(T_w-T)}{(T_w-T_i)}$
θ_b Dimensionless bulk temperature, $\frac{(T_w-T_b)}{(T_w-T_i)}$
ξ, η Transversal coordinates in computational plane

diameter of the duct with fins, a the semi-major axis of the elliptic duct, and X, Y, and Z two dimensionless transversal coordinates and one dimensionless axial coordinate, respectively. Taking advantage of the symmetry, only a quarter of the duct is used as the computational domain. The preceding equations are also subjected to the following boundary conditions:

$$W=0, \quad \theta=0 \qquad \text{on the wall of the duct and on the fins} \tag{4}$$

$$\frac{\partial W}{\partial n}=0, \quad \frac{\partial \theta}{\partial n}=0, \qquad \text{on the symmetrical line} \tag{5}$$

and

$$\theta=1, \quad Z=0 \tag{6}$$

Parameters of interest

The characteristics of fluid flow and heat transfer in the duct may be represented by the product of the friction factor and the Reynolds number, $f\mathrm{Re}$, the dimensionless bulk temperature, and the Nusselt number. For the purpose of comparing the results of the finned tube with the smooth tube (without fins), two different characteristic lengths are used here. One of them is the hydraulic diameter of the smooth elliptic duct without fins, D_{hs}, and the other is the hydraulic diameter of the elliptic duct with internal longitudinal fins, D_{hf}. These are defined as follows:

$$D_{\mathrm{hs}}=\frac{4A}{P} \tag{7}$$

$$D_{\mathrm{hf}}=\frac{4A}{P+4(H_a+H_b)} \tag{8}$$

where A and P represent the cross-sectional area and the perimeter of the elliptic duct, respectively. Now, defining $f\mathrm{Re}$, based on the above hydraulic diameters, one can write

$$(f\mathrm{Re})_s=\left(-D_{\mathrm{hs}}\frac{\frac{dp}{dz}}{\rho\frac{w_m^2}{2}}\right)\left(\frac{w_m D_{\mathrm{hs}}}{\nu}\right)=\frac{2}{W_m}\left(\frac{D_{\mathrm{hs}}}{a}\right)^2 \tag{9}$$

$$(f\mathrm{Re})_f=\left(-D_{\mathrm{hf}}\frac{\frac{dp}{dz}}{\rho\frac{w_m^2}{2}}\right)\left(\frac{w_m D_{\mathrm{hf}}}{\nu}\right)=\frac{2}{W_m}\left(\frac{D_{\mathrm{hf}}}{a}\right)^2 \tag{10}$$

and the local dimensionless bulk temperature is calculated by the following equation:

$$\theta_b(Z)=\frac{\int_A W\theta\, dA}{\int_A W\, dA}. \tag{11}$$

The two Nusselt numbers are defined as follows:

$$(\mathrm{Nu}_z)_s=-\frac{1}{4}\left(\frac{D_{\mathrm{hs}}}{D_{\mathrm{hf}}}\right)^2\frac{1}{\theta_b}\frac{d\theta_b}{dZ} \tag{12}$$

$$(\mathrm{Nu}_z)_f=-\frac{1}{4}\frac{1}{\theta_b}\frac{d\theta_b}{dZ} \tag{13}$$

where $(\mathrm{Nu}_z)_s$ and $(\mathrm{Nu}_z)_f$ are defined based on the hydraulic diameter of the smooth elliptic duct (without fins), D_{hs}, and on the hydraulic diameter of the elliptic duct with fins, D_{hf}, respectively.

Solution procedure

Grid generation

Due to the complexity of the finned elliptic duct, a numerically generated boundary-fitted coordinate system is applied to solve the difficulties with discretizing the computational domain and developing a general computer program. The basic idea of the boundary-fitted coordinate system is to have a coordinate system such that the computational domain boundary coincides with the coordinate lines. One of the methods often used in this type of analysis is suggested by Thompson[19] and Thomas and Middlecoff.[20] The grid point distribution is controlled according to this reference. Therefore, the domain transformation between physical coordinates (X, Y) and the boundary-fitted coordinates (ξ, η) is achieved by solving the two coupled system of equations:

$$\alpha\left(\frac{\partial^2 X}{\partial\xi^2}+\phi\frac{\partial X}{\partial\xi}\right)-2\beta\frac{\partial^2 X}{\partial\xi\,\partial\eta}+\gamma\left(\frac{\partial^2 X}{\partial\eta^2}+\psi\frac{\partial X}{\partial\eta}\right)=0 \tag{14}$$

$$\alpha\left(\frac{\partial^2 Y}{\partial\xi^2}+\phi\frac{\partial Y}{\partial\xi}\right)-2\beta\frac{\partial^2 Y}{\partial\xi\,\partial\eta}+\gamma\left(\frac{\partial^2 Y}{\partial\eta^2}+\psi\frac{\partial Y}{\partial\eta}\right)=0 \tag{15}$$

where

$$\alpha=\left(\frac{\partial X}{\partial\eta}\right)^2+\left(\frac{\partial Y}{\partial\eta}\right)^2, \tag{16}$$

$$\beta=\frac{\partial X}{\partial\xi}\frac{\partial X}{\partial\eta}+\frac{\partial Y}{\partial\xi}\frac{\partial Y}{\partial\eta}, \tag{17}$$

$$\gamma=\left(\frac{\partial X}{\partial\xi}\right)^2+\left(\frac{\partial Y}{\partial\xi}\right)^2, \tag{18}$$

$$\phi=-\frac{\frac{\partial X}{\partial\xi}\frac{\partial^2 X}{\partial\xi^2}+\frac{\partial Y}{\partial\xi}\frac{\partial^2 Y}{\partial\xi^2}}{\left(\frac{\partial X}{\partial\xi}\right)^2+\left(\frac{\partial Y}{\partial\xi}\right)^2} \tag{19}$$

$$\psi=-\frac{\frac{\partial X}{\partial\eta}\frac{\partial^2 X}{\partial\eta^2}+\frac{\partial Y}{\partial\eta}\frac{\partial^2 Y}{\partial\eta^2}}{\left(\frac{\partial X}{\partial\eta}\right)^2+\left(\frac{\partial Y}{\partial\eta}\right)^2}. \tag{20}$$

Equations 14 and 15 are solved by using the successive over relaxation (SOR) method subjected to a grid distribution given on the boundary. The resulting grid constructions in Figures 2a and 2b illustrate the grids in the physical plane (X, Y), and computational plane (ξ, η), respectively.

Finite difference

At this stage, it is necessary to transfer the governing equations 1 and 2 to the computational domain as

$$\frac{\partial}{\partial\xi}\left[\frac{1}{J}\left(\alpha\frac{\partial W}{\partial\xi}-\beta\frac{\partial W}{\partial\eta}\right)\right]+\frac{\partial}{\partial\eta}\left[\frac{1}{J}\left(\gamma\frac{\partial W}{\partial\eta}-\beta\frac{\partial W}{\partial\xi}\right)\right]+J=0, \tag{21}$$

and

$$JC\frac{\partial\theta}{\partial Z}=\frac{\partial}{\partial\xi}\left[\frac{1}{J}\left(\alpha\frac{\partial\theta}{\partial\xi}-\beta\frac{\partial\theta}{\partial\eta}\right)\right]+\frac{\partial}{\partial\eta}\left[\frac{1}{J}\left(\gamma\frac{\partial\theta}{\partial\eta}-\beta\frac{\partial\theta}{\partial\xi}\right)\right], \tag{22}$$

with

$$J=\frac{\partial X}{\partial\xi}\frac{\partial Y}{\partial\eta}-\frac{\partial X}{\partial\eta}\frac{\partial Y}{\partial\xi}, \tag{23}$$

where α, β, γ have the same definition as in Equations 16, 17,

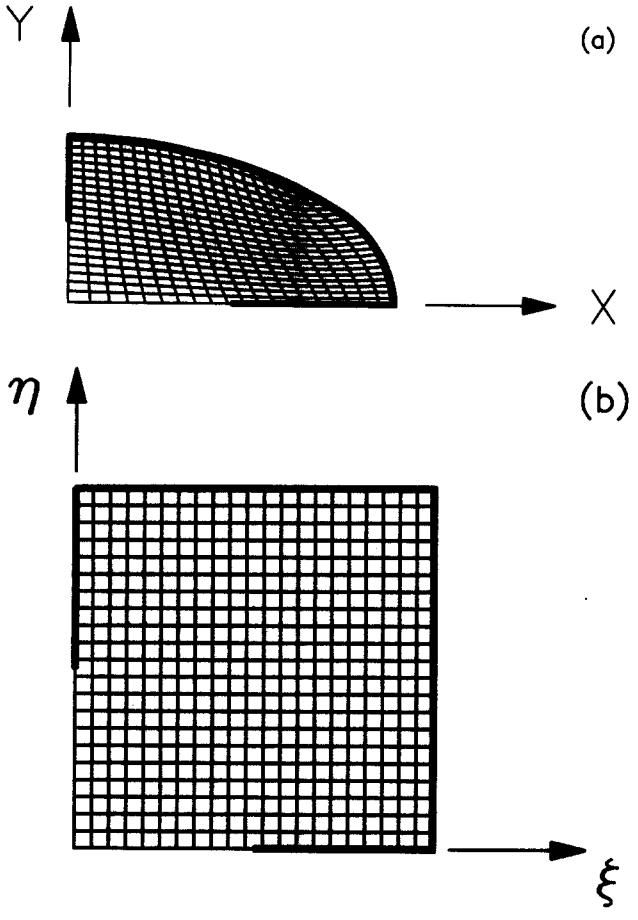

Figure 2 (a) Grid configuration in physical domain; (b) grid configuration in computational domain

and 18. Thus, by using a control volume-based finite difference procedure (Patankar[21]), the governing differential equations 21 and 22 are reduced to a set of algebraic equation systems. In the process, the nonlinear cross-derivative, $\partial^2/\partial\xi\,\partial\eta$, is treated as a source term. It is apparent that iteration is needed to obtain the solution. Since Equations 21 and 22 are not coupled, the momentum equation is solved first to find the velocity field, and then the 3-D energy equation with its parabolic properties is solved by the marching method. Also, due to the nonlinearity of the source term, several iterations are needed to obtain the temperature field in each marching step. The following convergence criterion was chosen for this study,

$$\frac{\|F_{i,j}^{k+1}-F_{i,j}^{k}\|_\infty}{\|F_{i,j}^{k+1}\|_\infty}\leq 10^{-5}, \tag{24}$$

where F refers to the dependent variable W or θ, respectively, k stands for the kth iteration, and $\|\cdot\|_\infty$ is the infinite norm. When the convergence temperature field is satisfied, the local bulk temperature and the Nusselt number are calculated from Equations 11 through 13.

To assure the accuracy of the results presented, numerical tests were performed for the elliptic duct to determine the effects of the grid size. The tabular results are given in Table 1. Comparison of these results with that given by Shah and London[6] indicates that for the cases considered here, the 21 × 21 grid is adequate. Therefore, the successive calculations are performed based on this grid size. The axial marching step size of $\Delta Z=0.00025$ is used in all the computations. The results obtained for the bulk temperature using the above marching step size deviates less than 0.1% compared with the axial marching step size of $\Delta Z=0.000125$. Additionally, all of the computations have been conducted on a Micro VAX 8800.

Results and discussion

The fully developed friction factors and the Nusselt numbers for the elliptic duct with fins are numerically calculated and documented in Table 2. Both $(f\mathrm{Re})_s$, $(f\mathrm{Re})_f$ and $(\mathrm{Nu})_s$, $(\mathrm{Nu})_f$ are given in this analysis for convenience. Also, the data shown in Table 2 are used to draw the curves in Figures 3 and 4, where the $(f\mathrm{Re})_s$ to $(f\mathrm{Re})_o$ ratio and the $(\mathrm{Nu})_s$ to $(\mathrm{Nu})_o$ ratio are presented graphically for different H^* and α^*. $(f\mathrm{Re})_o$ and $(\mathrm{Nu})_o$ refer to the corresponding case of the smooth elliptic duct without fins. Inspection of these curves indicates that the friction factor can be increased by increasing the relative fin height. It is also evident that the Nusselt number, $(\mathrm{Nu})_s$, increases and achieves a maximum value, and then decreases as the relative fin height increases. The maximum Nusselt number occurs around $H^*=0.8\sim0.9$ for all calculations with $\alpha^*=0.25$, 0.5, 0.8, 1.0. This behavior is, in fact, similar to the circular finned duct subjected to uniform heat flux boundary conditions.[6] For $\alpha^*=1$ and $H^*=0$ (circular duct case), the results obtained for $(f\mathrm{Re})_s=63.99$ and $(\mathrm{Nu})_s=3.670$ are in excellent agreement with the published values of 64 and 3.658, respectively.[6] For the case of $\alpha^*=1$ and $H^*=1$, the elliptic duct

Table 1 Grid independent test results

		$(f\mathrm{Re})$		
α^*	Grid	Present study	Shah and London[6]	Error (%)
0.25	21 × 21	72.21	72.16	0.058
	27 × 27	72.20	72.16	0.050
0.5	21 × 21	67.26	67.26	0.007
	31 × 31	67.27	67.26	0.003
0.8	21 × 21	64.36	64.39	0.054
	31 × 31	64.38	64.39	0.023
1.0	21 × 21	63.99	64.00	0.016
	31 × 31	64.00	64.00	0.00

Table 2 $(f\mathrm{Re})$ and Nu for fully developed flow

α^*	H^*	$(f\mathrm{Re})_s$	$(\mathrm{Nu})_s$	$(f\mathrm{Re})_f$	$(\mathrm{Nu})_f$
0.25	0.0	72.20	3.78	72.20	3.78
	0.5	108.61	3.78	45.36	1.58
	0.8	270.63	12.51	69.34	3.20
	0.9	301.73	16.04	71.53	3.80
	1.0	313.62	15.85	67.26	3.40
0.5	0.0	67.26	3.75	67.26	3.75
	0.5	133.29	4.97	50.02	1.86
	0.9	297.78	16.31	68.78	3.76
	1.0	309.20	16.11	61.71	3.21
0.8	0.0	64.33	3.67	64.33	3.67
	0.5	135.53	5.36	50.72	2.00
	0.9	291.06	16.19	67.34	3.74
	1.0	303.38	15.96	58.91	3.10
1.0	0.0	63.99	3.67	63.99	3.67
	0.5	140.57	5.60	51.46	2.05
	0.9	294.18	16.14	65.89	3.61
	1.0	301.82	15.96	58.40	3.09

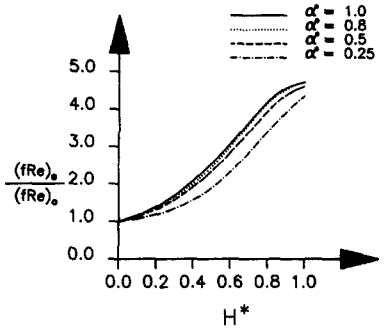

Figure 3 Variation $\frac{(fRe)_s}{(fRe)_o}$ with H^*

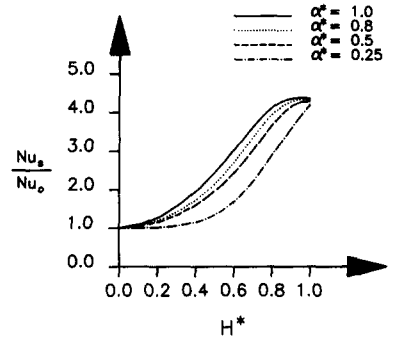

Figure 4 Variation $\frac{(Nu)_s}{(Nu)_o}$ with H^*

reduces to the circular sector duct and the results obtained for $(fRe)_f = 58.406$ and $(Nu)_f = 3.09$ agree well with the published results of 59.074 and 3.055, respectively, as obtained by Trupp and Lau.[22]

A comparison of the present results for the fully developed Nusselt number with Soliman[12] for the special case of the circular duct ($\alpha^* = 1$) and relative fin heights of $H^* = 0.2$, 0.4, 0.6, 0.7, 0.8 is documented in Table 3. Inspection of the data in this table indicates very close agreement between the two studies at a low relative fin height, H^*, that deviates at a higher H^*. This difference is mainly due to the fact that our results consider zero thickness for the fin, whereas Soliman[12] used the fin thickness of $\beta = \pi/60$ RAD.

Generally, the thermal entrance length is equal to the distance from the entrance of the duct to the downstream location where the local Nusselt number is 1.05 times the fully developed value, as defined by Shah and London.[6] This definition is used in the present study. Table 4 presents values for the estimated thermal entrance length for the elliptic duct with four internal longitudinal fins. Also presented in this table are the effect of the minor- to major-axis ratio, α^*, and the relative fin height, H^*.

The following section is a summary of the results for the entrance region of the elliptic duct with internal fins. The variation of the local Nusselt number, Nu_z, in the entrance region of the circular duct for $H^* = 0$ is displayed in Figure 5. Comparison of the results obtained with those given by Shah and London[6] and Soliman[12] indicates close agreement. Also shown in Figure 5 is a comparison of the present results for the circular duct with relative fin heights of $H^* = 0.2$, 0.4, 0.8 with Soliman.[12] Further inspection of this figure indicates an excellent agreement between the two studies. This figure is provided here only to further verify the validity of the present method.

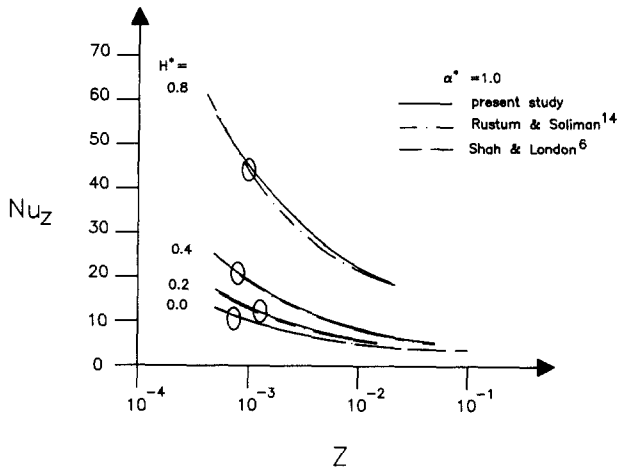

Figure 5 Local Nusselt number for a circular duct

For the finned elliptic duct, the bulk temperature, θ_b, and local Nusselt numbers, $(Nu_z)_s$ and $(Nu_z)_f$, are computed in the development region of the elliptic duct with internal longitudinal fins from Equations 11 through 13, respectively. The variations of the local bulk temperature, θ_b, isotherm lines, and the variation of the local Nusselt number, Nu_z, of some cases are displayed in Figures 6 through 11. As expected, the bulk temperature decreases from unity in the inlet to zero (0) as the axial distance increases. The Nusselt number is very large in the entrance region, and it decreases as the axial distance increases, approaching asymptotically the fully developed value. Included in these results are the effects of relative fin heights, as well as the ratio of minor-axis to major-axis of the elliptic duct.

Figure 6 represents the variation of the bulk temperature against the axial position for $\alpha^* = 0.8$. The effects of the relative fin height is illustrated by showing results for $H^* = 0.5$, 0.9, 1.0. A similar situation occurs in the other cases. The lines of the isotherms at two different axial positions for $\alpha^* = 0.25$ and $H^* = 0.5$ are illustrated in Figures 7a and 7b. These are provided to determine the influence of the fin on the temperature field. Five isotherm loops of $\theta = 0.17$, 0.33, 0.5, 0.67, and 0.83, at axial distance $Z = 0.0125$, are shown in Figure 7a. Another five isotherm loops of $\theta = 0.15$, 0.29, 0.44, 0.58, and 0.73, at axial

Table 3 Comparison of Nu for the circular duct ($\alpha^* = 1.0$)

	Nu	
H^*	Present study	Soliman[12]
0.2	3.760	3.819
0.4	4.466	4.770
0.6	7.550	8.930
0.7	12.250	14.770
0.8	15.996	16.090

Table 4 Estimate of the thermal entrance length, L_f^*, for the elliptic duct with four fins

	L_f^*			
α^*	$H^* = 0$	$H^* = 0.5$	$H^* = 0.9$	$H^* = 1.0$
0.25	0.0846	0.095	0.102	0.107
0.5	0.044	0.100	0.0532	0.0596
0.8	0.0343	0.0994	0.0424	0.0471

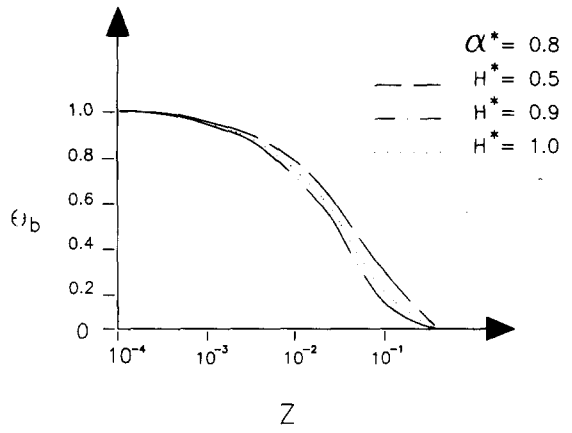

Figure 6 Local bulk temperature for $\alpha^* = 0.8$

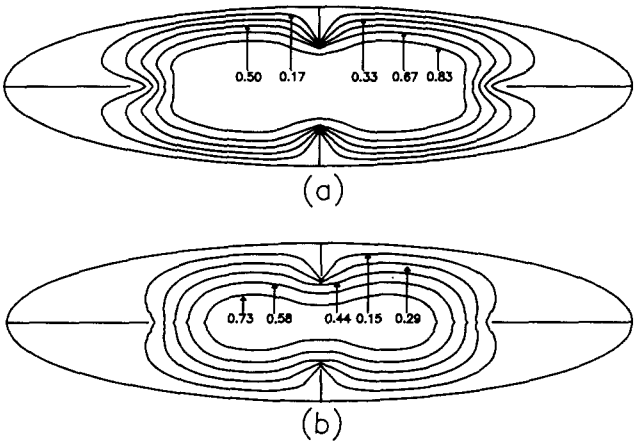

Figure 7 (a) Isotherm for $Z = 0.0125$, $\alpha^* = 0.25$, $H^* = 0.5$; (b) isotherm for $Z = 0.0625$, $\alpha^* = 0.25$, $H^* = 0.5$

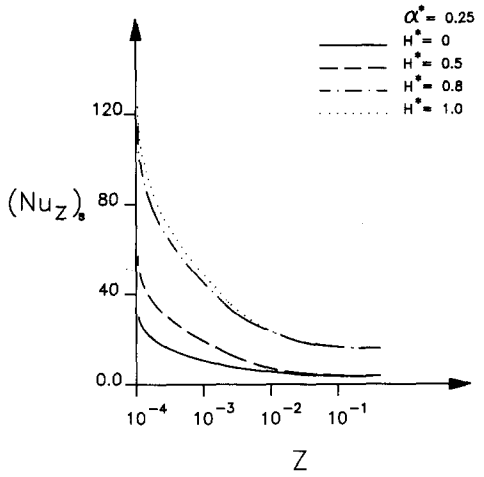

Figure 8 Local Nusselt number $(Nu_z)_s$ for $\alpha^* = 0.25$

distance $Z = 0.0625$, are presented in Figure 7b. It is evident that the temperature field is influenced seriously by the attached fins. The isotherms are no longer of elliptic shape, but become irregular. It is further observed that the inlet effect decreases as the axial distance increases.

Figures 8 through 10 show the variation of the local Nusselt number, $(Nu_z)_s$, against the entrance length, Z, for $\alpha^* = 0.25$, 0.5, 0.8, and a combination of different relative fin heights. It is seen that $(Nu_z)_s$ decreases from a high value near the entrance to the fully developed value at a greater axial distance, which is also presented in Table 2. It is also seen that the fully developed

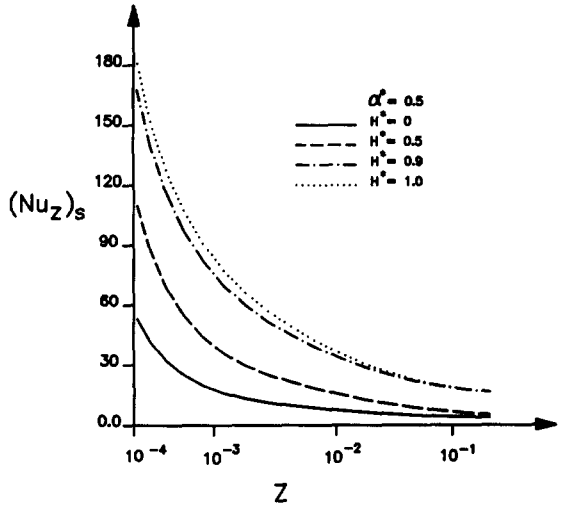

Figure 9 Local Nusselt number $(Nu_z)_s$ for $\alpha^* = 0.5$

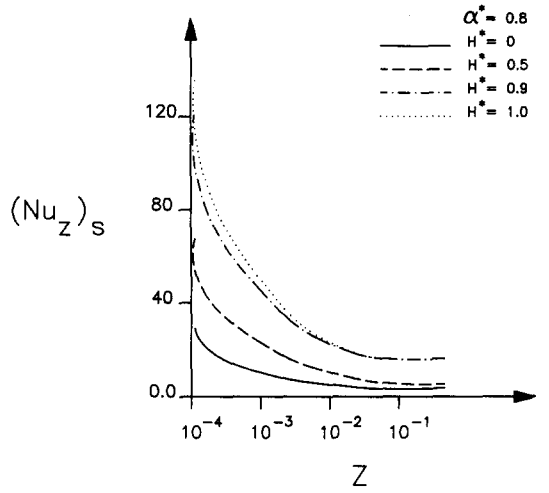

Figure 10 Local Nusselt number $(Nu_z)_s$ for $\alpha^* = 0.8$

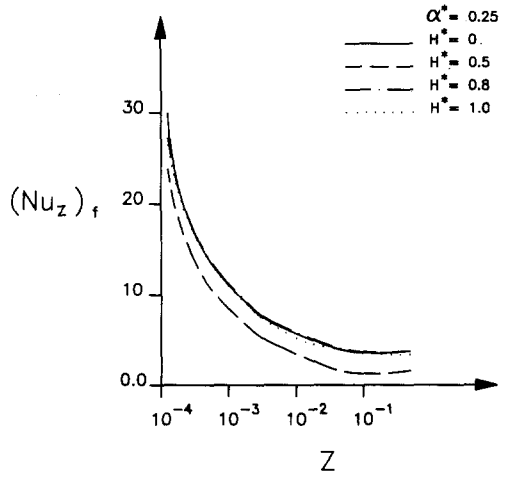

Figure 11 Local Nusselt number $(Nu_z)_f$ for $\alpha^* = 0.25$

Nusselt number, $(Nu)_s$, for the finned elliptic duct is four times higher than that given for the smooth elliptic duct (without fins) in different cases. Figure 11 displays the variation of the local Nusselt number, $(Nu_z)_f$, as defined in Equation 13 with axial distance for the case of $\alpha^* = 0.25$. The Nusselt number behavior, decreasing with increasing axial distance, holds for different fin heights. However, it is not easy to estimate the effects of the relative fin height in this figure. Therefore, $(Nu_z)_s$ is suitable for comparing the results for the finned elliptic duct with those for the smooth elliptic duct (without fins).

Concluding remarks

Convective heat transfer in the elliptic duct with four internal longitudinal fins is analyzed numerically for various combinations of relative fin heights and minor-axis to major-axis ratios in the elliptic duct. The fins are considered continuous and of zero thickness. The boundary-fitted coordinate is used to solve the difficulty induced by the computational domain. Thermal developed and developing heat transfers with a laminar fully developed velocity field and a comparison with the available literature are obtained and presented in this article. The results indicate that there exists an optimum relative fin height that gives a maximum heat transfer coefficient at a given value of α^*. The bulk temperature and the Nusselt number variation with axial distance are illustrated graphically. As expected, a large heat transfer coefficient in the entrance region is obtained, approaching asymptotically the fully developed value at a greater axial distance where the Nusselt number, $(Nu)_s$, for the finned elliptic duct is four times higher than that for the smooth elliptic duct without fins in different cases.

Acknowledgment

The results presented in this article were obtained in the course of research sponsored by the Department of Energy under Subcontract No. 19X-SE133V.

References

1 Eckert, E. R. G., Goldstein, R. G., Pfender, E., Ibele, W. E., Patankar, S. W., Ramsey, S. V., Simon, T. W., Decker, N. A., Kuehn, T. H., Lee, H. O., and Girshick, S. L. Heat transfer—a review of the 1985 literature. *Int. J. Heat Mass Transfer*, 1986, **29**, 1767–1842

2 Eckert, E. R. G., Goldstein, R. G., Pfender, E., Ibele, W. E., Patankar, S. W., Ramsey, S. V., Simon, T. W., Decker, N. A., Kuehn, T. H., Lee, H. O., and Girshick, S. L. Heat transfer—a review of the 1986 literature. *Int. J. Heat Mass Transfer*, 1987, **30**, 2449–2523

3 Eckert, E. R. G., Goldstein, R. G., Pfender, E., Ibele, W. E., Patankar, S. W., Ramsey, S. V., Simon, T. W., Decker, N. A., Kuehn, T. H., Lee, H. O., and Girshick, S. L. Heat transfer—a review of the 1987 literature. *Int. J. Heat Mass Transfer*, 1988, **31**, 2401–2488

4 Eckert, E. R. G., Goldstein, R. G., Pfender, E., Ibele, W. E., Patankar, S. V., Simon, T. W., Decker, N. A., Lee, H. O., Girshick, S. L., Scott, C. J., Strykowski, P. J., and Tamma, K. K. Heat transfer—a review of the 1988 literature. *Int. J. Heat Mass Transfer*, 1989, **32**, 2211–2280

5 Kakac, S., Shah, R. K., and Aung, W. *Handbook of Single-Phase Convection Heat Transfer*, Wiley Interscience, New York, 1987

6 Shah, R. K. and London, A. L. *Laminar Flow Forced-Convection in Ducts*, Supplement 1 to *Advances in Heat Transfer*, Academic Press, New York, 1978

7 Soloukhin, R. I. and Martynenko, O. G. Heat and mass transfer bibliography—Soviet literature. *Int. J. Heat Mass Transfer*, 1983, **26**, 1771–1781

8 Martynenko, O. G. Heat and mass transfer bibliography—Soviet literature. *Int. J. Heat Mass Transfer*, 1988, **31**, 2489–2503

9 Hu, M. H. and Chang, Y. P. Optimization of finned tubes for heat transfer in laminar flow. *J. Heat Transfer*, 1973, **3**, 332–338

10 Nandakumar, K. and Masliyah, J. H. Fully developed viscous flow in internally finned tubes. *Chem. Eng. J.*, 1985, **10**, 113–120

11 Soliman, H. M. and Feingold, A. Analysis of fully developed laminar flow in internally finned tubes. *Chem. Eng. J.*, 1977, **14**, 119–128

12 Soliman, H. M., Chau, T. S., and Trupp, A. C. Analysis of laminar heat transfer in internally finned tubes with uniform outside wall temperature. *J. Heat Transfer*, 1980, **102**, 598–604

13 Prakash, C. and Liu, Y. D. Analysis of laminar flow and heat transfer in the entrance region of an internally finned circular duct. *J. Heat Transfer*, 1985, **107**, 84–91

14 Rustum, I. M. and Soliman, H. M. Numerical analysis of laminar forced convection in the entrance region of tubes with longitudinal internal fins. *J. Heat Transfer*, 1988, **110**, 310–313

15 Zhang, H. Y., Ebadian, M. A., and Campo, A. Flow and thermal analysis of laminar forced-convection in the entrance region of semi-circular duct with longitudinal internal fins. *1990 AIAA/ASME Thermophys. Heat Transfer Conf.*, 1990, **HTD-137**, 165–172

16 Tao, L. N. On some laminar forced-convection problems. *ASME J. Heat Transfer*, 1961, **83**, 466–472

17 Schenk, J. and Han, B. S. Heat transfer from laminar flow in ducts with elliptic cross section. *Appl. Sci. Res.*, 1967, **17**, 96–114

18 Ebadian, M. A., Topakoglu, H. C., and Arnas, O. A. On the convective heat transfer in a tube of elliptic cross-section maintained under constant wall temperature. *J. Heat Transfer*, 1986, **108**, 33–39

19 Thompson, J. F., Thames, F., and Martin, C. Automatic numerical generation of body-filled curvilinear coordinate system for field containing any number of arbitrary two-dimensional bodies. *J. Comp. Phys.*, 1974, **24**, 299–319

20 Thomas, P. and Middlecoff, J. Direct control of grid point distribution in meshes generated by elliptic equations. *AIAA J.*, 1982, **18**, 652–656

21 Patankar, S. V. *Numerical Heat Transfer and Fluid Flow*, Hemisphere, Washington, DC, 1980

22 Trupp, A. C. and Lau, A. C. Y. Fully developed laminar heat transfer in circular sector ducts with isothermal walls. *J. Heat Transfer*, 1984, **106**, 467–469